JOURNAL OF GUIDANCE, CONTROL, AND DYNAMICS
Vol. 19, No. 1, January–February 1996

Nonlinear Control of Dual-Spin Spacecraft During Despin Through Precession Phase Lock

R. J. Kinsey
The Aerospace Corporation, Los Angeles, California 90009
D. L. Mingori
University of California, Los Angeles, Los Angeles, California 90024
and
R. H. Rand
Cornell University, Ithaca, New York 14853

When a dual-spin spacecraft is placed on orbit, thrusters bring the rotor and platform to an all spun condition. Then, during despin an internal torque motor aligned with the main bearing is activated to increase the rotor rate and decrease the platform rate, until the platform rate is near zero. We focus on the capture dynamics of precession phase lock, a phenomenon that can prevent successful despin. A spacecraft model used to illustrate precession phase lock contains an axially symmetric, dynamically unbalanced rotor. During precession phase lock, the unbalanced rotor becomes synchronized with the inertial free precession of the spacecraft. If the despin motor torque is constant and small relative to unbalance size, then precession phase lock causes a large secular deviation of the bearing axis from its desired direction. One common despin strategy to avoid this is to apply constant torque at the maximum capability of a relatively large motor. An alternative based on nonlinear closed-loop feedback control of despin motor torque, exploiting a priori knowledge of states favorable for despin through precession phase lock, is developed. Computer simulations demonstrate that this strategy can lead to successful despin when constant torque cannot—even with relatively limited motor torque.

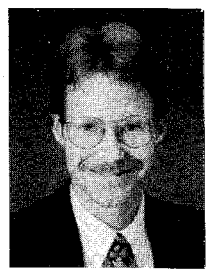

Robert J. Kinsey received his Bachelor's degree in physics and mathematics from the California State University at Fresno in 1980. He received his M.S. in engineering and Ph.D. in aerospace engineering from the University of California, Los Angeles, in 1983 and 1991, respectively. He is currently an Engineering Specialist at the Aerospace Corporation, where he has analyzed satellite control system stability and performance since 1983. His research interests are in nonlinear dynamics and control.

D. Lewis Mingori received his B.S. degree from the University of California, Berkeley, in 1960, his M.S. from the University of California, Los Angeles (UCLA), in 1962, and his Ph.D. from Stanford University (Aeronautics and Astronautics) in 1966. From 1966 to 1968 he was a member of the technical staff of The Aerospace Corporation, and since 1968 he has been a faculty member at UCLA. His teaching and research are in the areas of dynamics and control with applications primarily in the aerospace field. His research interests include spacecraft attitude control, spinning and dual-spin spacecraft dynamics, gravity-stabilized satellites, spinning rockets, control of flexible space structures, model reduction, and robust control.

Richard H. Rand did his undergraduate work at Cooper Union and got his masters and doctorate from Columbia University. He has been a professor in the Department of Theoretical and Applied Mechanics at Cornell University since 1967. He has published widely in nonlinear dynamics and associated perturbation methods, as well as in biomathematics. He worked with coauthors Kinsey and Mingori during a sabbatical at the University of California, Los Angeles, in 1990.

Received March 27, 1993; revision received June 12, 1995; accepted for publication Aug. 27, 1995.

Introduction

A DUAL-SPIN spacecraft consists of two bodies connected through a bearing assembly that allows relative rotation between the bodies. The first body, referred to as the rotor, spins about the axis of relative rotation, providing gyroscopic stiffness that helps to maintain the desired spacecraft attitude. The second body, referred to as the platform, is inertially nonrotating; it provides a support base for pointing payloads, such as a directional antenna. Since the late 1950s, tens of dual-spin spacecraft have been flown successfully. Typically, the largest of these weigh on the order of a ton and have roughly cylindrical dimensions on the order of 10 ft in diameter by 25 ft in height.

An idealized dual-spin spacecraft with a dynamically unbalanced rotor is shown in Fig. 1. The platform (body A) and rotor (body B) share a common axis $\hat{b}_3$, about which relative rotation is possible. We refer to $\hat{b}_3$ as the spin axis or the bearing axis. Let the inertial angular velocities of A and B be expressed as

$$\underline{\omega}^A = \omega_1\hat{b}_1 + \omega_2\hat{b}_2 + \omega_A\hat{b}_3 \tag{1}$$

$$\underline{\omega}^B = \omega_1\hat{b}_1 + \omega_2\hat{b}_2 + \omega_B\hat{b}_3 \tag{2}$$

where $\hat{b}_1$, $\hat{b}_2$, and $\hat{b}_3$ are unit vectors fixed in B as shown in Fig. 1. When a dual-spin spacecraft is placed on orbit, a series of thruster maneuvers bring the spacecraft to an all spun condition in which the platform and rotor rotate together with zero relative rate (i.e., $\omega_A = \omega_B$) and the spacecraft has sizeable angular momentum $\underline{h}$. Then an internal torque motor, referred to as the despin motor, is activated to provide torque to reduce ω_A and increase ω_B. This paper focuses on spacecraft dynamic behavior during this despin maneuver. Despin is complete when $\omega_A = 0$ and ω_B has reached its desired nonzero value. Figure 2 depicts the simulated behavior of ω_A and ω_B during a normal despin maneuver. The simulation is begun with the spacecraft in an all spun condition (point A). The rotor spins up and the platform spins down until the platform is despun (point B).

No thrusting is done during despin, and since environmental torques are negligibly small, the direction of $\underline{h}$ remains inertially fixed and its magnitude remains constant. The deviation of the direction of the spin axis from the fixed direction of $\underline{h}$ is denoted by θ and referred to as the cone angle (see Fig. 1). When θ is nonzero, a coning motion occurs in which the spin axis precesses about $\underline{h}$. The coning rate λ_0 is referred to as the inertial free precession rate. A more precise definition of λ_0 will be given later in Eq. (10).

Three different types of capture phenomena that can prevent a dual-spin spacecraft from successfully completing its despin maneuver have been observed on orbit. These include minimum energy trap, nutation resonance, and precession phase lock (PPL). The minimum energy trap occurs when the relative rotation rate between the platform and rotor is near zero and the despin motor is unable to produce sustained relative rotation.[1-3]

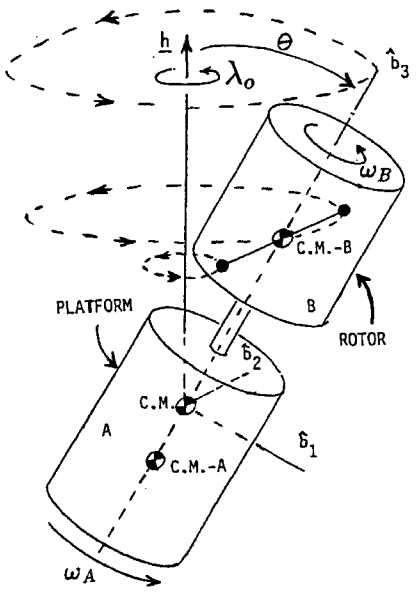

Fig. 1 Idealized unbalanced dual-spin spacecraft.

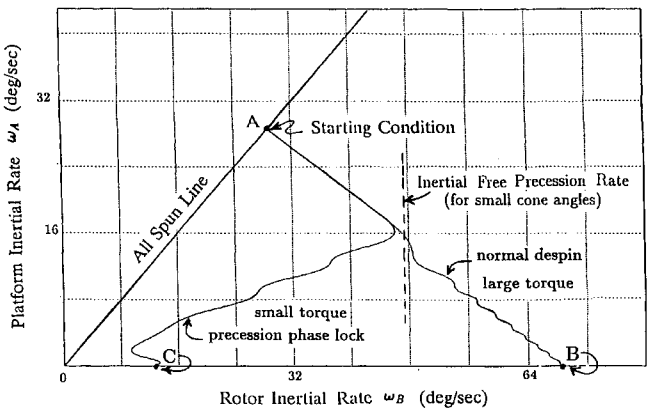

Fig. 2 Despin dynamics of an unbalanced dual-spin spacecraft.

The nutation resonance occurs when the relative rotation rate is near a critical nonzero value and the despin motor is unable to increase the relative rate significantly beyond this value. It is characterized by violent oscillations of the cone angle about a slowly growing mean value. The nutation resonance is caused by dynamic effects due to the combination of a dynamic unbalance on one body (either platform or rotor) and an asymmetry on the other body, in conjunction with limited motor torque capability.[1,3-6]

This paper focuses on spacecraft dynamic behavior during PPL. What distinguishes PPL from nutation resonance is that PPL is caused by dynamic effects due solely to a dynamic unbalance on one body. The spacecraft shown in Fig. 1 has the minimum complexity necessary of PPL to occur. Let I^A and I^B be the inertia matrices for the platform (body A) and the rotor (body B), for axes parallel to $\hat{b}_1$, $\hat{b}_2$, and $\hat{b}_3$, which are units vectors fixed in body B and passing through the system c.m. I^A is assumed to have the form

$$I_A = \begin{bmatrix} I^A_{11} & 0 & 0 \\ 0 & I^A_{11} & 0 \\ 0 & 0 & I^A_{33} \end{bmatrix} \tag{3}$$

From Eq. (3) we see that A is symmetrical and dynamically balanced for $\hat{b}_1$, $\hat{b}_2$, and $\hat{b}_3$. I^B is assumed to have the form

$$I_B = \begin{bmatrix} I^B_{11} & 0 & I^B_{13} \\ 0 & I^B_{11} & 0 \\ I^B_{13} & 0 & I^B_{33} \end{bmatrix} \tag{4}$$

From Eq. (4) we see that B is also symmetrical in the sense that the moments of inertia for $\hat{b}_1$ and $\hat{b}_2$ are equal. However, B is dynamically unbalanced due to the presence of a nonzero product of inertia. We assume that the mass centers of A and B both lie on the $\hat{b}_3$ axis.

In Fig. 1, the paths of the unbalance and the spin axis during PPL are depicted with dashed lines. PPL occurs when the rotor inertial spin rate ω_B is near the spacecraft inertial free precession rate λ_0. The motion of the rotor unbalance becomes synchronized with the precession of the spacecraft. The spin axis component of spacecraft angular momentum decreases, and the transverse component increases. As this happens, a slow secular growth in the cone angle θ occurs. Adams[3] uses computer simulation results to illustrate attitude motion during PPL. Lebsock et al.[7] analyze PPL subject to the constraint that ω_B increases linearly during rotor spinup, i.e., they assume constant torque and also neglect small nonlinear dynamic effects due to PPL that inhibit rotor spinup. They solve the linearized equations of motion analytically in terms of confluent hypergeometric functions. This leads to expressions that relate the size of the rotor unbalance, the despin torque magnitude, the initial momentum

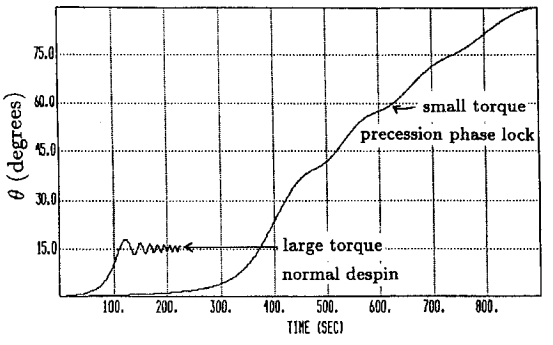

Fig. 3 Cone angle θ during despin.

state, and the cone angle following the despin maneuver. Without neglecting small nonlinear effects as in Ref. 7, Kinsey et al.[8] develop a method by which the final cone angle may be estimated analytically as a function of the spacecraft mass properties (including the size of the rotor unbalance) and the despin motor torque magnitude. Reference 9 contains a preliminary version of the current work involving nonlinear control during passage through PPL resonance.

Figure 2 depicts the simulated behavior of ω_A and ω_B during two despin scenarios: normal despin and an extreme example of PPL. Constant despin motor torque is used in both cases, but the torque magnitude is larger in the normal despin case. The mass and inertia properties of the platform and (unbalanced) rotor are the same in the two cases. Furthermore, both simulations are begun with the spacecraft in an all-spun condition (point A). In the normal despin case with larger torque, the rotor spins up and the platform spins down until the platform rate is zero (point B). During the process, the cone angle θ remains near zero, as desired (see Fig. 3). The behavior during PPL is depicted in the smaller torque case. This case begins as before, but when the rotor rate reaches the inertial free precession rate, the behavior changes markedly. Both the rotor rate and the platform rate decrease toward zero, and the spin axis momentum is transferred into transverse coning motion. By the time the platform rate reaches zero (point C), θ has increased to a large value and the spacecraft is essentially tumbling end-over-end. These cases represent two extremes. The normal despin case occurs when the torque is large relative to the unbalance. The PPL case occurs when the torque is small relative to the unbalance. If the torque is intermediate, then moderate growth in the cone angle will occur as the spacecraft passes through the PPL condition.

In the design of dual-spin spacecraft, a number of factors provide strong motivation to use a despin motor with limited torque capability and to accept small degree of rotor unbalance. There are virtually always severe weight, size, and power limitations on hardware components, such as a despin motor. Once despin is achieved, relatively small torque is required to overcome friction and maintain the desired rotor rate. Accurate balancing of the rotor is technically difficult as well as costly. Virtually every dual-spin spacecraft has some residual rotor unbalance, even after balancing efforts. Therefore, PPL during despin must be considered in the design process.

One common despin strategy is to apply nearly constant torque at the maximum capability of a relatively large motor. In this paper, we develop an alternative strategy in which the despin motor provides a time-varying torque governed by a closed-loop feedback control law. We demonstrate through analysis and computer simulation that this strategy as opposed to a constant torque can produce successful despin through PPL with a relatively small motor and without excessive cone angle growth.

Equations of Motion

Consider the idealized unbalanced dual-spin spacecraft shown in Fig. 1. A despin torque motor applies a torque $\underline{N}$ to the rotor and an equal and opposite torque to the platform. The spacecraft is assumed to be free from external torques, so that its angular momentum $\underline{h}$ has constant magnitude and remains fixed in inertial space. Both of the spacecraft bodies are assumed to be completely rigid (no energy dissipation).

To obtain a set of governing equations, one can first formulate an expression for the angular momentum of the system using Eqs. (1–4). Using I_1 to denote $I_{11}^A + I_{11}^B$, this yields

$$\underline{h} = \left(I_1\omega_1 + I_{13}^B\omega_B\right)\hat{\boldsymbol{b}}_1 + I_1\omega_2\hat{\boldsymbol{b}}_2 + \left(I_{33}^A\omega_A + I_{33}^B\omega_B + I_{13}^B\omega_1\right)\hat{\boldsymbol{b}}_3 \quad (5)$$

Since no external forces act, one may differentiate this angular momentum and set the result equal to zero to obtain the following three equations:

$$I_1\dot{\omega}_1 + I_{13}^B\dot{\omega}_B = -\omega_2\left(I_{33}^A\omega_A + I_{33}^B\omega_B - I_1\omega_B\right) - I_{13}^B\omega_1\omega_2 \quad (6)$$

$$I_1\dot{\omega}_2 = \omega_1\left(I_{33}^A\omega_A + I_{33}^B\omega_B - I_1\omega_B\right) + I_{13}^B\left(\omega_1^2 - \omega_B^2\right) \quad (7)$$

$$I_{33}^A\dot{\omega}_A + I_{33}^B\dot{\omega}_B + I_{13}^B\dot{\omega}_1 = I_{13}^B\omega_2\omega_B \quad (8)$$

A fourth equation is obtained by differentiating the angular momentum of A alone and setting the $\hat{\boldsymbol{b}}_3$ component of the result equal to N, the despin torque. This yields

$$I_{33}^A\dot{\omega}_A = -N \quad (9)$$

Equations (6–9) constitute the governing equations for the system.

Introduce the following scaled variables and dimensionless parameters:

$$\bar{\omega}_1 = \frac{\omega_1}{\omega_A(0)} \qquad \bar{\omega}_2 = \frac{\omega_2}{\omega_A(0)}$$

$$\bar{\omega}_A = \frac{\omega_A}{\omega_A(0)} \qquad \bar{\omega}_B = \frac{\omega_B}{\omega_A(0)}$$

$$\nu = I_{13}^B/I_1 \qquad \sigma = I_{33}^B/I_1$$

$$J = \frac{I_{33}^A}{I_{33}^B} \qquad \tau = \omega_A(0)t \qquad ()' = \frac{\mathrm{d}}{\mathrm{d}\tau} \quad (10)$$

$$L = \frac{N}{\omega_A^2(0)}\left(\frac{1}{I_{33}^A} + \frac{1}{I_{33}^B}\right)$$

$$\lambda_0 = \frac{I_{33}^A\omega_A + I_{33}^B\omega_B}{I_1\omega_A(0)} = \sigma J\bar{\omega}_A + \sigma\bar{\omega}_B$$

Using Eqs. (10), the following equations can be obtained from Eqs. (6–9):

$$\bar{\omega}_1' + \nu\bar{\omega}_B' = \bar{\omega}_2(\bar{\omega}_B - \lambda_0) - \nu\bar{\omega}_1\bar{\omega}_2 \quad (11)$$

$$\bar{\omega}_2' = -\bar{\omega}_1(\bar{\omega}_B - \lambda_0) + \nu\left(\bar{\omega}_1^2 - \bar{\omega}_B^2\right) \quad (12)$$

$$\sigma\bar{\omega}_B' + \nu\bar{\omega}_1' = \nu\bar{\omega}_2\bar{\omega}_B + [\sigma JL/(1+J)] \quad (13)$$

$$\bar{\omega}_A' = -L/(1+J) \quad (14)$$

In what follows, we assume initial conditions corresponding to a state of steady spin about a principal axis when the despin motor torque L is zero and the relative rate between bodies A and B is also zero. From Eqs. (11–14), these conditions are

$$\bar{\omega}_1(0) = \frac{[1-\sigma(1+J)] + \sqrt{[1-\sigma(1+J)]^2 + 4\nu^2}}{2\nu} \quad (15)$$

$$\bar{\omega}_2(0) = 0 \quad (16)$$

$$\bar{\omega}_B(0) = 1 \quad (17)$$

$$\bar{\omega}_A(0) = 1 \quad (18)$$

Equations (11–14) together with initial conditions (15–18) form a complete set of dimensionless exact equations of motion for the spacecraft.

If we let h_t and h_a denote the magnitudes of the transverse and spin axis components of the spacecraft angular momentum, then the cone angle is defined as

$$\theta = \tan^{-1}(h_t/h_a) \quad (19)$$

From Eqs. (5), (10), and (19), we obtain

$$\theta = \tan^{-1}\left[\frac{\sqrt{\bar{\omega}_1^2 + \bar{\omega}_2^2 + 2\nu\bar{\omega}_1\bar{\omega}_B + \nu^2\bar{\omega}_B^2}}{\sigma J\bar{\omega}_A + \sigma\bar{\omega}_B + \nu\bar{\omega}_1}\right] \tag{20}$$

Equation (20) is an exact expression for the cone angle based on the dimensionless parameters and variables defined in Eq. (10).

Averaged Equations

In Eqs. (11–18) and (20), ν, σ, J, and L are dimensionless parameters where L is the relative size of the despin motor torque, σ and J are the spacecraft mass properties, and ν is the size of the rotor dynamic unbalance. In what follows, we assume that ν is a small parameter ($\ll 1$). Since we are interested in cases for which L is limited, we also assume that $L = \nu K$, where K is a dimensionless parameter of $\mathcal{O}(1)$. The function $f(\nu)$ is said to be $\mathcal{O}[g(\nu)]$ if there are positive constants M and ν_0 such that

$$|f(\nu)| \leq M|g(\nu)| \qquad \text{for all} \qquad |\nu| \leq \nu_0$$

In the remainder of this development, terms of $\mathcal{O}(\nu^2)$ are neglected. Under these assumptions, Eqs. (11–18) may be simplified through algebraic manipulation and by truncating terms of $\mathcal{O}(\nu^2)$. The simplified equations and initial conditions are

$$\bar{\omega}_1' = \bar{\omega}_2(\bar{\omega}_B - \lambda_0) - \nu\bar{\omega}_1\bar{\omega}_2 \tag{21}$$

$$\bar{\omega}_2' = -\bar{\omega}_1(\bar{\omega}_B - \lambda_0) + \nu\left(\bar{\omega}_1^2 - \bar{\omega}_B^2\right) \tag{22}$$

$$\bar{\omega}_B' = \frac{\nu K J}{1+J} + \frac{\nu\lambda_0\bar{\omega}_2}{\sigma} \tag{23}$$

$$\bar{\omega}_A' = (-\nu K)/(1+J) \tag{24}$$

$$\bar{\omega}_1(0) = \frac{\nu}{[\sigma(1+J)-1]} \tag{25}$$

$$\bar{\omega}_2(0) = 0 \tag{26}$$

$$\bar{\omega}_B(0) = 1 \tag{27}$$

$$\bar{\omega}_A(0) = 1 \tag{28}$$

Now, derive an expression for the spacecraft angular momentum for its c.m. Define $\bar{\underline{h}}$, a scaled momentum vector, as

$$\bar{\underline{h}} = \frac{\underline{h}}{\omega_A(0)I_1} = (\bar{\omega}_1 + \nu\bar{\omega}_B)\hat{\boldsymbol{b}}_1 + (\bar{\omega}_2)\hat{\boldsymbol{b}}_2 + (\lambda_0 + \nu\bar{\omega}_1)\hat{\boldsymbol{b}}_3 \tag{29}$$

Using the initial conditions (25–28), the following magnitude is obtained:

$$\bar{h} = \sigma(1+J) + \mathcal{O}(\nu) \tag{30}$$

Equations (29) and (30) can be used to obtain

$$\bar{\omega}_1^2 + \bar{\omega}_2^2 + \lambda_0^2 = \sigma^2(1+J)^2 + \mathcal{O}(\nu) \tag{31}$$

Next, introduce the following nonlinear coordinate transformation (note that λ_0 is not constant):

$$u = \lambda_0\bar{\omega}_2$$

$$v = \lambda_0\bar{\omega}_1 \tag{32}$$

$$w = \bar{\omega}_B - \lambda_0$$

Substituting Eqs. (32) into Eqs. (21–24) yields Eqs. (33–35). Substitutions have been made for λ_0 from Eqs. (10), and for $\bar{\omega}_1^2 + \bar{\omega}_2^2$ using Eq. (31):

$$u' = -wv + \nu F_0 \tag{33}$$

$$F_0 = \frac{J\bar{\omega}_A}{\gamma}\left[\sigma^2(1+J)^2 - \frac{2J^2\bar{\omega}_A^2}{\gamma^2}\right] + \frac{w}{\gamma}\left[\sigma^2(1+J)^2 - \frac{2J^2\bar{\omega}_A^2}{\gamma}\left(1+\frac{3}{\gamma}\right)\right] - \frac{w^2J\bar{\omega}_A}{\gamma}\left(1+\frac{4}{\gamma}+\frac{6}{\gamma^2}\right) - \frac{w^3}{\gamma}\left(1+\frac{2}{\gamma}+\frac{2}{\gamma^2}\right)$$

$$v' = wu \tag{34}$$

$$w' = [\nu KJ/(1+J)] + \nu\gamma u \tag{35}$$

where $\gamma = (1/\sigma) - 1$.

The F_0 term in Eq. (33) may be simplified through use of the method of averaging,[10] here applied via the following near-identity transformation:

$$\bar{u} = u \tag{36}$$

$$\bar{v} = v - \nu G_0 \tag{37}$$

$$G_0 = \frac{\sigma^2(1+J)^2}{\gamma} - \frac{2J^2\bar{\omega}_A^2}{\gamma^2}\left(1+\frac{3}{\gamma}\right) - \frac{wJ\bar{\omega}_A}{\gamma}\left(1+\frac{4}{\gamma}+\frac{6}{\gamma^2}\right) - \frac{w^2}{\gamma}\left(1+\frac{2}{\gamma}+\frac{2}{\gamma^2}\right)$$

$$\bar{w} = w \tag{38}$$

Substituting Eqs. (36–38) into Eqs. (33–35) and neglecting terms of $\mathcal{O}(\nu^2)$ that arise when G_0 is differentiated, we obtain

$$\bar{u}' = -\bar{w}\bar{v} + \nu F_1 \tag{39}$$

$$\bar{v}' = \bar{w}\bar{u} \tag{40}$$

$$\bar{w}' = [\nu KJ/(1+J)] + \nu\gamma\bar{u} \tag{41}$$

where

$$F_1 = \frac{J\bar{\omega}_A}{\gamma}\left[\sigma^2(1+J)^2 - \frac{2J^2\bar{\omega}_A^2}{\gamma^2}\right] \qquad \gamma = \frac{1}{\sigma} - 1$$

From Eqs. (24) and (28), we have

$$\bar{\omega}_A = [-\nu K\tau/(1+J)] + 1 \tag{42}$$

The initial conditions for Eqs. (39–41) are

$$\bar{u}(0) = 0 \tag{43}$$

$$\bar{v}(0) = \frac{(\nu J/\gamma)[\sigma^2(1+J)^2 - (2J^2/\gamma^2)]}{[1-\sigma(1+J)]} \tag{44}$$

$$\bar{w}(0) = 1 - \sigma(1+J) \tag{45}$$

Equations (39–45) form a complete set of averaged equations of motion.

Behavior Near Resonance

Recall from Eqs. (32) and (38) that $\bar{w} = \bar{\omega}_B - \lambda_0$, where $\bar{\omega}_B$ and λ_0 are the normalized rotor rate and precession rate, respectively. When $\bar{w} = 0$, the rotor rate equals the precession rate, and PPL resonance can occur. We next determine several conditions the system parameters must satisfy in order for resonance to occur, and then we examine a modified set of equations that describe behavior near resonance.

To determine when $\bar{w}$ can reach 0, expand $\bar{w}$ using the definition for λ_0 in Eqs. (10) to obtain

$$\bar{w} = \bar{\omega}_B - \sigma(\bar{\omega}_B + J\bar{\omega}_A)$$

Since $\bar{\omega}_A$, $\bar{\omega}_B$, and J are all >0, σ must be <1 for $\bar{w}$ to reach 0. Further, we consider only cases for which $\bar{w}$ is <0 at time 0 and

passes through 0 prior to the completion of the despin maneuver. Thus, from Eq. (45), $\sigma(1+J)$ must be >1. For physically realizable spacecraft, $\sigma(1+J)$ must be <2. And since real spacecraft tend to have values of $\sigma(1+J)$ closer to 1, we restrict our attention (somewhat arbitrarily) to $\sigma(1+J) < 1.4$.

Now consider Eqs. (39–41) when $\bar{w} = 0$. The equations become

$$\bar{u}' = \nu F_1 \tag{46}$$

$$\bar{v}' = 0 \tag{47}$$

$$\bar{w}' = [\nu K J/(1+J)] + \nu\gamma\bar{u} \tag{48}$$

In the remainder of this development, we assume without loss of generality that $\nu > 0$. Then in Eq. (48), noting that $\gamma = (1/\sigma) - 1 > 0$ (because $\sigma < 1$), the growth of $\bar{w}$ will be inhibited to the extent that $\bar{u}$ is negative. We have found through computer simulations that $\bar{u}$ remains small until $\bar{w}$ is near 0, and then $\bar{u}$ grows negative. In Eq. (46), the behavior of $\bar{u}$ is governed by the term νF_1. Since ν is assumed to be a positive constant, the value of F_1 near $\bar{w} = 0$ is the key factor that causes $\bar{u}$ to grow negative and, consequently, inhibits the growth of $\bar{w}$.

To determine a lower bound for F_1, suppose that the growth of $\bar{w}$ proceeds linearly until $\bar{w}$ reaches 0. Then the soonest time, τ_1, at which $\bar{w}$ could reach 0, can be calculated using Eqs. (41) and (45) and neglecting the $\nu\gamma\bar{u}$ term in Eq. (41). This calculation yields

$$\tau_1 = \frac{(1+J)[\sigma(1+J) - 1]}{\nu K J} \tag{49}$$

Substitute from Eq. (49) into Eq. (42) to obtain the value of $\bar{\omega}_A$ at time τ_1.

$$\bar{\omega}_A(\tau_1) = \frac{(1+J)(1-\sigma)}{J} \tag{50}$$

Note that $\bar{\omega}_A$ decreases linearly from 1 to 0 (as a consequence of the assumed symmetry of the platform), so that the value in Eq. (50) is an upper bound for $\bar{\omega}_A$ when $\bar{w}$ reaches 0. Substitute from Eq. (50) into the definition of F_1 given with Eq. (39) to obtain a value for F_1 at τ_1,

$$F_1(\tau_1) = -\sigma^3(1+J)^3 \tag{51}$$

Recall that by definition, σ and J are positive. Note that in Eq. (39), F_1 becomes less negative as $\bar{\omega}_A$ decreases. Thus, the value in Eq. (51) is a lower bound for F_1 at $\bar{w} = 0$.

Note that F_1 is slowly time varying since it is a function of $\bar{\omega}_A$, which is slowly time varying. In general, we have found through computer simulations that the performance of the control strategy described in the next section is not highly sensitive to slow variations in F_1. Thus, for convenience we replace F_1 with a constant by substituting from Eq. (51) into Eqs. (39–41) to obtain

$$\bar{u}' = -\bar{w}\bar{v} - \nu\sigma^3(1+J)^3 \tag{52}$$

$$\bar{v}' = \bar{w}\bar{u} \tag{53}$$

$$\bar{w}' = [\nu K J/(1+J)] + \nu\gamma\bar{u} \tag{54}$$

These equations are useful for gaining insight into cone angle growth when the system is near resonance (i.e., near $\bar{w} = 0$). Recall from Eq. (32) that $\bar{u}$ and $\bar{v}$ are proportional to the normalized transverse rate components $\bar{\omega}_2$ and $\bar{\omega}_1$, respectively. And from Eq. (20), $\bar{\omega}_1$ and $\bar{\omega}_2$ are primary contributors to the cone angle θ. Thus, θ will be relatively small when $\bar{u}$ and $\bar{v}$ are small, and θ will be relatively large when either $\bar{u}$ or $\bar{v}$ is large (or both).

If one starts from the initial conditions given in Eqs. (43–45) and applies a constant motor torque, the solution of the averaged equations (39–41) will evolve toward some particular point $(\bar{u}_p, \bar{v}_p, 0)$ in the $(\bar{u}, \bar{v}, \bar{w})$ space. The location of this point depends on the relative magnitude of the motor torque and the inertial properties of the system. It is useful to determine how the final cone angle is related to the particular point $(\bar{u}_p, \bar{v}_p, 0)$ achieved. Once this information is known, one can attempt to vary the motor torque to make the trajectory pass through a more desirable point. Thus, the next step in the development is to map out the characteristics of trajectories that start from various points in the $(\bar{u}, \bar{v}, 0)$ plane. Equations (52–54) are useful for constructing this map.

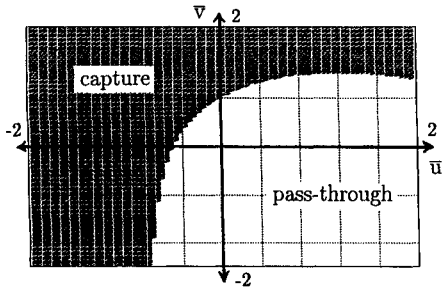

Fig. 4 Pass-through region at resonance.

From extensive computer simulation results, we have found that starting from an initial point $(\bar{u}_p, \bar{v}_p, 0)$ and letting time increase indefinitely in Eqs. (52–54), the system will exhibit one of two types of behavior. In the first, $\bar{w}$ passes relatively quickly through 0 as it increases nearly linearly. We refer to this as pass through. In the second, $\bar{w}$ stalls near 0 and remains captured near it indefinitely. We refer to this as capture. Whether capture or pass through occurs depends entirely on the initial point chosen. By comparing the value of $\bar{w}$ obtained by numerically integrating Eqs. (52–54) over a relatively long period of time with the value it would have if it increased linearly, points for which pass through occurs can be isolated. These points form the region that the control strategy needs to reach. This is because pass through in Eqs. (52–54) corresponds to nearly linear growth of $\bar{w}$ and relatively small growth of $\bar{u}$ and $\bar{v}$ in Eqs. (39–41). This in turn corresponds to relatively small cone angle growth during despin. Note that in Eqs. (39–41) pass through cannot be distinguished from capture in general because of the time-varying term F_1, and so these equations cannot be used to find desirable regions.

Figure 4 was generated through extensive numerical integration of Eqs. (52–54) (12,800 computer simulation runs) with the following system parameters: $\nu = 0.008$, $\sigma = 0.536$, $J = 1.612$, $L = 0.0064$. These parameters correspond to $\sigma(1+J) = 1.40$ and $\gamma = (1/\sigma) - 1 = 0.87$. Each run was long enough so that $\bar{w}$ would reach 4 if it increased linearly. If $\bar{w}$ exceeded 3 during the run, we concluded that pass through had occurred. Otherwise, we concluded that $\bar{w}$ was captured near 0. Figure 4 depicts the region of points $(\bar{u}, \bar{v}, 0)$ for which pass through occurred. We refer to this region as a hole in the resonance plane at $\bar{w} = 0$. The hole is valid only for the particular system chosen, but this figure will serve as an example for the remainder of this paper. For another system with a different despin motor torque capability or different inertias, the shape and size of the hole will vary from that shown in Fig. 4.

Control Strategy

We neglect all processing delays and assume that the despin torque motor has an ideal (unity) transfer function. We further assume that the inertial spin axis rate components of the platform and the rotor and the transverse rate components of the spacecraft are all measurable and available. Under these assumptions, the states $\bar{u}$, $\bar{v}$, $\bar{w}$ in the averaged equations can be calculated from measured variables. In real spacecraft, there may not be sensors available to directly measure all of these rates. In that case, it would be necessary to construct an estimator to approximate the true rates from available measurements. In many cases, the described approach does not require highly accurate knowledge of rates, and so estimated rates should suffice.

In a few cases in which the hole in the resonance plane is relatively small, more accurate rate knowledge is needed to determine when the system trajectory is within the hole, which is critical for the success of the control strategy to be described. Because of the cost of adding hardware to measure rates, this strategy may not be the best approach in those cases.

Our control strategy, which follows, drives the system trajectory into and through the hole in the resonance plane. Begin with the (steady spin) initial conditions (15–18), and apply the maximum

possible constant torque L_{max}. Continue using constant torque until large-amplitude cone angle growth occurs, i.e., until $\sqrt{(u^2 + v^2)}$ reaches a large value, which indicates that the system is near resonance. Then switch from constant torque to the feedback control law given in the next paragraph. For the system described in the preceding section, computer simulation results suggest that a suitable time to switch from constant torque to feedback control is when $\sqrt{(u^2 + v^2)}$ first exceeds 0.4. In general, the value of $\sqrt{(u^2 + v^2)}$ at which the switch is commanded should be chosen on a case-by-case basis so that w is close to zero but not positive when the switch occurs. Note that it is not necessary to use the averaged variables $\bar{u}$, $\bar{v}$, and $\bar{w}$ to determine when to switch to feedback control, and using u, v, and w simplifies the computations.

To develop a feedback control law, we first apply the polar coordinate transformation

$$\bar{u} = r\sin(\chi) \tag{55}$$

$$\bar{v} = r\cos(\chi) \tag{56}$$

to the averaged equations (39–41). This leads to

$$r' = \nu F_1 \sin(\chi) \tag{57}$$

$$\chi' = -\bar{w} + (\nu F_1/r)\cos(\chi) \tag{58}$$

$$\bar{w}' = [\nu K J/(1 + J)] + \nu\gamma r \sin(\chi) \tag{59}$$

Differentiate Eq. (58) and substitute r' from Eq. (57) and $\bar{w}'$ from Eq. (59) into the result. Recall that $\nu K = L$. Assuming that the system is near resonance, i.e., $\bar{w}$ is $\mathcal{O}(\nu)$, and neglecting terms of $\mathcal{O}(\nu^2)$, we have

$$\chi'' + \nu\gamma r \sin(\chi) = -[LJ/(1 + J)] \tag{60}$$

$$r' = \nu F_1 \sin(\chi) \tag{61}$$

Equation (60) is a pendulum type equation with slowly varying frequency. When L is a small constant (corresponding to limited constant despin motor torque), PPL resonance has a large effect. During PPL resonance, χ oscillates about a negative offset value between -90 and 0 deg, and r grows [since $F_1 < 0$ and $\sin(\chi) < 0$].

For the example system, the hole in the resonance plane (Fig. 4) is relatively large, but is not reached using constant torque starting from the (steady spin) initial conditions (15–18). To bring the system trajectory into the hole, we apply a feedback control law that causes (unstable) growing oscillations in χ. This control law is

$$L = -L_{max}\chi' \tag{62}$$

Note that $r = \sqrt{(\bar{u}^2 + \bar{v}^2)} = \mathcal{O}(1)$ and $F_1 = \mathcal{O}(1)$. From the assumption that $\bar{w} = \mathcal{O}(\nu)$, we have from Eq. (58) that $\chi' = \mathcal{O}(\nu)$, so L defined in Eq. (62) never exceeds L_{max}. In fact, the control law in Eq. (62) tends to under utilize the available torque, and in some cases despin takes a relatively long time to reach completion. If need be, this may be remedied by using 2 or 3 times L_{max} in Eq. (62).

The expression for χ' is obtained from the definition of F_1 given with Eq. (39) and Eq. (58),

$$\chi' = -\bar{w} + \frac{\nu J\bar{\omega}_A}{\gamma r}\left[\sigma^2(1 + J)^2 - \frac{2J^2\bar{\omega}_A^2}{\gamma^2}\right]\cos(\chi) \tag{63}$$

Since $r = \sqrt{(\bar{u}^2 + \bar{v}^2)}$ and $\cos(\chi) = \bar{v}/r$, Eq. (63) may be written as

$$\chi' = -\bar{w} + \frac{\nu J\bar{\omega}_A\bar{v}}{\gamma(\bar{u}^2 + \bar{v}^2)}\left[\sigma^2(1 + J)^2 - \frac{2J^2\bar{\omega}_A^2}{\gamma^2}\right] \tag{64}$$

From the near-identity transformation (36–38), we have that $u \equiv \bar{u}$ and $w \equiv \bar{w}$, and $v = \bar{v}$ to $\mathcal{O}(1)$. Thus, neglecting terms of $\mathcal{O}(\nu^2)$, Eq. (64) may be rewritten as

$$\chi' = -w + \frac{\nu J\bar{\omega}_A v}{\gamma(u^2 + v^2)}\left[\sigma^2(1 + J)^2 - \frac{2J^2\bar{\omega}_A^2}{\gamma^2}\right] \tag{65}$$

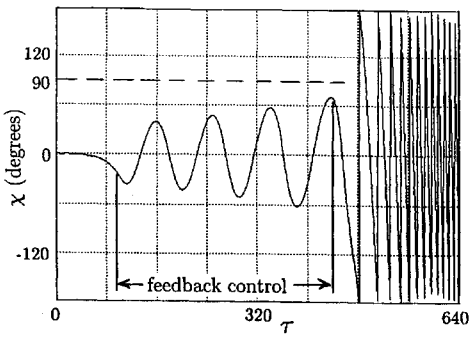

Fig. 5 Behavior of χ with feedback control.

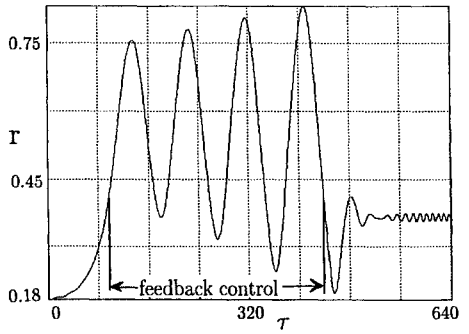

Fig. 6 Behavior of r with feedback control.

This is the expression for χ' used to implement Eq. (62) in computer simulations of the control strategy.

When L is substituted from Eq. (62) into Eq. (60), the result is

$$\chi'' - L_{max}[J/(1 + J)]\chi' + \nu\gamma r \sin(\chi) = 0 \tag{66}$$

The negative damping in Eq. (66) causes growing oscillations in χ. (See Fig. 5 for the behavior of the example system.) We allow these oscillations to continue until the system trajectory is well within the hole in the resonance plane. To ensure that the trajectory stays in the hole long enough after the switch to constant torque, we also require that χ be near a peak value at the time of switching, so that χ' is near zero. It is not critical that χ' be right at 0. The goal is to avoid χ' so large that the trajectory moves out of the hole before it has moved sufficiently far through the resonance plane. Also, note in Eq. (58) that χ' becomes negative as $\bar{w}$ grows positive following passage through resonance. Thus, in cases for which the hole in the resonance plane is relatively small, it is desirable to switch to constant torque when χ has peaked at its largest positive value still within the hole. This maximizes the time that the trajectory is within the hole while still near resonance.

One more important factor in deciding when to switch to constant torque is the behavior of $r = \sqrt{(\bar{u}^2 + \bar{v}^2)}$, which indicates the relative size of the cone angle. (See Fig. 6 for the behavior of the example system.) When χ is between 0 and 180 deg, from Eq. (61) we have that $r' < 0$, which means that the cone angle is decreasing. If we switch to constant torque when χ has just peaked at a large value between 90 and 180 deg, then r will have been decreasing for some length of time, and so the cone angle will be relatively small. Computer simulation results suggest that in addition to χ being near a peak value within the hole, waiting for r to drop to a relatively low level can help minimize the cone angle following the switch to constant torque.

Returning to the example system, the switch back to the maximum possible constant torque is made when χ is near 90 deg, $\chi' < 0.08$, and $r < 0.4$. After the switch, passage through resonance is achieved with a relatively small cone angle, as shown in Fig. 7. For this case, using constant torque alone (no feedback) leads to a final cone angle of 73 deg.

The whole sequence for the example system is shown in Fig. 8, which depicts the system trajectory in a three-dimensional space of points $(\bar{u}, \bar{v}, \bar{w})$. With no rotor unbalance and zero initial cone angle,

Table 1 Mean cone angle at despin, θ_m: constant torque vs feedback control

System parameters, dimensionless						θ_m, deg	
ν	σ	J	L	$\sigma(1+J)$	γ	Constant torque	Feedback control
0.002	0.247	4.102	0.0016	1.26	3.05	83	3
0.003	0.213	5.291	0.0041	1.34	3.69	76	4
0.004	0.342	2.363	0.0036	1.15	1.92	68	6
0.005	0.755	0.854	0.0025	1.40	0.32	69	9
0.006	0.410	2.195	0.0066	1.31	1.44	57	6
0.007	0.167	6.290	0.0032	1.22	4.99	88	7
0.008	0.536	1.612	0.0064	1.40	0.87	73	11
0.009	0.290	3.034	0.0016	1.17	2.45	89	8
0.010	0.578	1.230	0.0048	1.29	0.73	80	8
0.010	0.167	5.586	0.0016	1.10	4.99	89	15

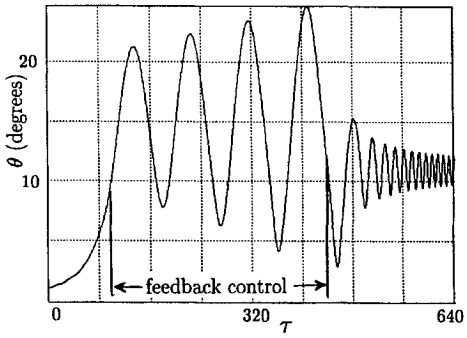

Fig. 7 Behavior of θ with feedback control.

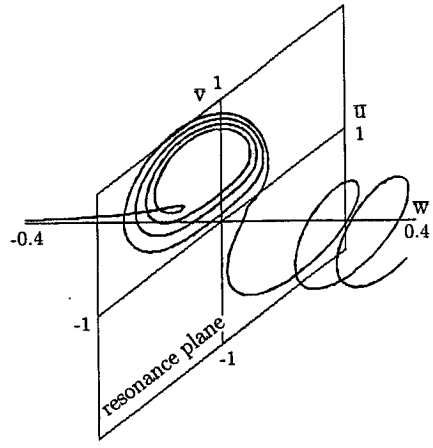

Fig. 8 Trajectory in $(\bar{u}, \bar{v}, \bar{w})$ space with feedback control.

the trajectory would move straight along the $\bar{w}$ axis. In the example system, the trajectory starts to move away from the $\bar{w}$ axis as the resonance plane is approached. The switch is made from constant torque to feedback control when $\sqrt{(u^2 + v^2)}$ exceeds 0.4, which is about the same time that $r = \sqrt{(\bar{u}^2 + \bar{v}^2)}$ also exceeds 0.4. Then, the trajectory begins to spiral above the $\bar{w}$ axis while remaining near the resonance plane. When the trajectory is near $\chi = 90$ deg, $r < 0.4$, and χ has just reached a peak (i.e., the trajectory has "turned a corner"), a switch is made back to the maximum available constant torque. The system then pokes through the hole in the resonance plane. The spiraling around the $\bar{w}$ axis that occurs after that corresponds to a relatively small cone angle near 11 deg. These results were obtained from numerical integration of the exact equations of motion, with the control law implemented as already described.

Numerical Verification

In the case of constant despin motor torque, computer simulation results indicate that the mean cone angle following despin θ_m is inversely related to the torque L. When L is very small relative to unbalance size (represented by ν), θ_m is nearly 90 deg and the spacecraft tumbles nearly end-over-end. When L is large relative to ν, then θ_m is nearly zero, and the spacecraft spin axis is nearly aligned with the direction of its angular momentum vector $\bar{h}$. When L has an intermediate value relative to ν, θ_m has an intermediate value between zero and 90 deg. In cases for which a small constant L results in θ_m large (e.g., above 40 deg), our control strategy can be used to achieve a significantly smaller θ_m.

Computer simulations have been used to study a variety of parameter sets (ν, σ, J, L) to verify the effectiveness of this control strategy. In these studies, it was assumed that added complexity associated with a feedback control system is not warranted unless θ_m is relatively large when constant torque is used. With this in mind, we considered only points for which θ_m exceeds 40 deg for constant torque. The feedback control strategy was applied to the exact equations of motion (11–14) that were numerically integrated in order to obtain θ_m. Table 1 summarizes simulation results. In general, using the feedback control strategy as opposed to constant torque leads to a significantly smaller value of the mean cone angle following despin, θ_m.

Summary

Through extensive numerical investigation, we can determine that there is a region of states near resonance for which passage through resonance can be achieved even though motor torque is quite limited. This region is not entered when constant torque is applied starting from at rest initial conditions. The dynamic behavior of the spacecraft near resonance can be described by a pendulum type equation. This paper develops a control strategy that employs closed-loop feedback control of motor torque when the system is near resonance. The choice of feedback control law has the effect of adding negative damping to the pendulum type equation, resulting in dynamic behavior that drives the system toward the pass-through region.

We have demonstrated numerically that this control stretegy is effective for despin of a dual-spin spacecraft through precession phase lock (PPL) resonance. For a given despin motor with limited torque capability, using this control strategy as opposed to constant torque leads to a significantly smaller mean cone angle following despin. This result has practical significance in the design of dual-spin spacecraft.

Acknowledgments

R. J. Kinsey sincerely thanks the Aerospace Corporation for its partial financial support of this work through an Advanced Study Grant. He also gratefully acknowledges the Lord Jesus Christ, the One through whom and for whom the world—with its wonderfully complex dynamics—was made.

References

[1]Scher, M. P., and Farrenkopf, R. L., "Dynamic Trap States of Dual-Spin Spacecraft," *AIAA Journal*, Vol. 12, No. 12, 1974, pp. 1721–1725.

[2]Hollars, M. G., "Minimum Energy Trap States of Dual-Spin Spacecraft," *Journal of Guidance, Control, and Dynamics*, Vol. 5, No. 3, 1982, pp. 286–290.

[3]Adams, G. J., "Dual-Spin Spacecraft Dynamics During Platform Spinup," *Journal of Guidance and Control*, Vol. 3, No. 1, 1980, pp. 29–36.

[4]Cochran, J. E., "Nonlinear Resonances in the Attitude Motion of Dual-Spin Spacecraft," *Journal of Spacecraft and Rockets*, Vol. 14, No. 9, 1977, pp. 562–572.

[5]Cochran, J. E., and Beaty, J. R., "Near-Resonant and Transition Attitude Motion of a Class of Dual-Spin Spacecraft," *Journal of the Astronautical Sciences*, Vol. 26, No. 1, 1978, pp. 19–45.

[6]Or, A. C., "Resonances in the Despin Dynamics of Dual-Spin Spacecraft," *Journal of Guidance, Control, and Dynamics*, Vol. 14, No. 2, 1991, pp. 321–329.

[7]Lebsock, K. L., McEnnan, J. J., and Murphy, J. R., "Despin Through Unity Inertia Ratio," *Journal of the Astronautical Sciences*, Vol. 30, No. 3, 1982, pp. 213–227.

[8]Kinsey, R. J., Mingori, D. L., and Rand, R. H., "Spinup Through Resonance of Rotating Unbalanced Systems with Limited Torque," *AIAA/AAS Astrodynamics Conference* (Portland, OR), AIAA, Washington, 1990, pp. 805–813 (AIAA Paper 90-2966).

[9]Kinsey, R. J., Mingori, D. L., and Rand, R. H., "Nonlinear Controller to Reduce Resonance Effects During Despin of a Dual-Spin Spacecraft Through Precession Phase Lock," *Proceedings of the 31st Conference on Decision and Control*, Vol. 4, Inst. of Electrical and Electronic Engineers, Piscataway, NJ, 1992, pp. 3025–3030 (IEEE Paper 92-506).

[10]Sanders, J. A., and Verhulst, F., *Averaging Methods in Nonlinear Dynamical Systems*, Vol. 59, Applied Mathematical Sciences, Springer–Verlag, New York, 1985, Chap. 5, pp. 83–123.